A Chemical Reaction Model for Physical Vapor Deposition of Compound Semiconductor Films

A model for the physical vapor deposition of compound semiconductor films that describes film growth from component molecular beams is presented. Constitutive relationships are used in the model to account for incomplete adsorption from the incident molecular beams, emission of adsorbed components into vacuum, and surface reactions of the elemental species. The model predicts film composition and growth rate as a function of incident fluxes and substrate temperature. It is applicable for important binary and ternary alloy semiconductors including the II-VI and III-V compounds over the range of deposition conditions yielding both stoichiometric and two-phase films. In this paper the model equations and the behavior predicted by the model are described for a number of material systems including (CdHg)Te, (CdZn)S, and $CuInSe_2$.

S. C. Jackson, B. N. Baron, R. E. Rocheleau and T. W. F. Russell
Institute of Energy Conversion
University of Delaware
Newark, DE 19716

Introduction

Thin-film compound semiconductors including the II-VI and III-V materials are used in photovoltaic cells (Russell et al., 1979), photonic devices (Mino et al., 1985), and thin-film transistors for large area display (Brody, 1984). This wide range of applications is the result of the high light absorption of such semiconductors and their ability to be controlled and adjusted for energy gap and refractive index using ternary alloys.

Physical vapor deposition (PVD) techniques including molecular beam epitaxy (MBE), vacuum evaporation, sputtering, electron beam evaporation, and hot wall evaporation are frequently used to deposit these compound semiconductors. A comprehensive review of physical vapor techniques can be found in Bunshah et al. (1982). Physical vapor deposition is best characterized by a comparison to chemical vapor deposition. While surface reactions can be very important for both deposition techniques, the manner in which film precursors are delivered to the substrate distinguishes these two techniques. In physical vapor deposition, the film precursors are generated and delivered to the film using a physical process. That is, the film precursors are generated from an independently controlled source separated from the substrate. The sources are typically an evaporation cell (a Knudsen cell or open boat). The film precursors are transported to the substrate by a molecular or atomic beam in high vacuum.

In chemical vapor deposition, however, gas phase reactions initiated by light, heat, or high-energy electrons (plasma) generate the film precursors typically in close proximity to the substrates. Gas phase and surface reactions may be closely coupled with the potential of significant heat and mass transport effects.

In this paper, a chemical reaction engineering model for the growth of binary and ternary compound semiconductor films from component molecular beams is described. This quantitative mathematical description provides a methodology for analyzing and understanding the laboratory-scale deposition process in order to guide materials research and the design of commercial production units.

Physical Situation

Physical vapor deposition techniques utilize molecular beams directed onto a temperature-controlled substrate upon which the species adsorb and react to deposit a film. In molecular beam epitaxy and vacuum evaporation the molecular beams are generated from individually heated compound or elemental sources. Figure 1 shows a representative thermal evaporation system with effusion-type sources. Evaporated materials flow from the source bottles, exit the collimating nozzles into vacuum, and

Correspondence concerning this paper should be addressed to R. E. Rocheleau.
S. C. Jackson is with the Engineering Department, E. I. duPont deNemours & Co., Wilmington, DE 19898.

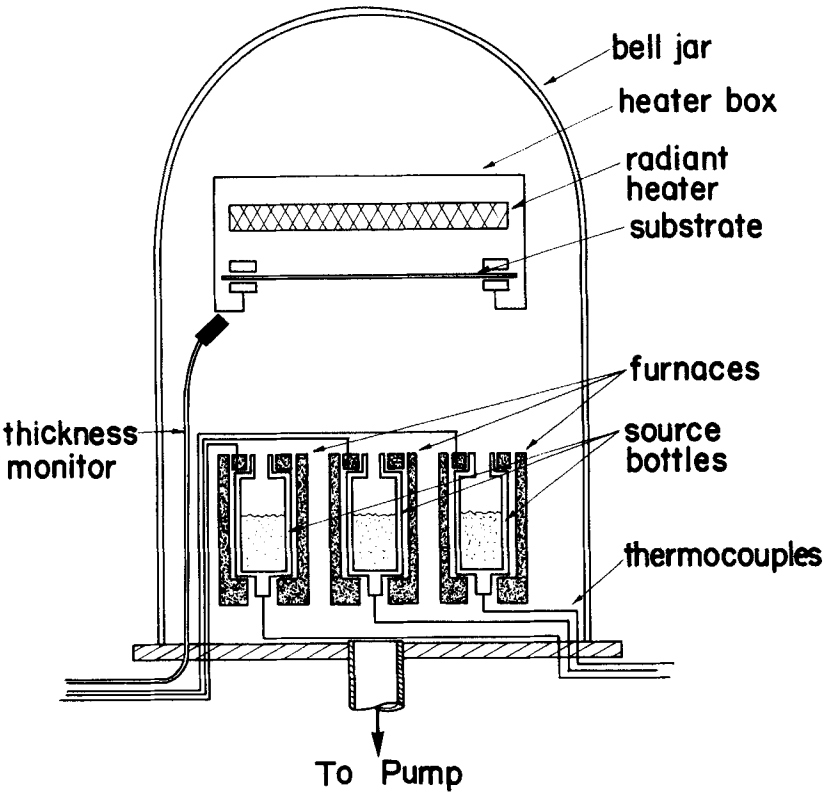

Figure 1. Typical vacuum system components for a three-source system.

form beams of evaporant atoms or molecules. At the pressures used in physical vapor deposition (less than 10^{-6} Pa) the evaporant material experiences few intermolecular collisions. The molecular flux or beam intensity at any surface within the system depends on the spatial distribution of the beam, the orientation of the surface toward the source, the source-to-surface distance, and the total mass flow from the source (Dayton, 1961; Stickney et al., 1968; Giordmaine and Wang, 1960; Jackson et al., 1985).

The growth of compound thin films from component molecular beams has been described by many investigators (Gunther, 1968; Smith and Pickhardt, 1975; Faurie et al., 1983, 1985; Chow and Johnson, 1985; Jansen and Melnyk, 1984; Foxon, 1983; Kawabe and Matsiura, 1984; Myers et al., 1982; Summers et al., 1984) with general agreement that the conversion or utilization of one species and the film composition vary with the substrate temperature and flux of the other components. A simplified description of the generally accepted mechanisms that explain this behavior follows.

The substrate suspended over the sources intercepts material from the component beams. The incident molecules will either be reflected or be adsorbed. The fraction reflected depends on the energy of the incident species and the thermal accommodation characteristics of the substrate. The adsorbed species, generally considered to be adatoms, can diffuse to favorable low-energy sites and react, or can be emitted into vacuum. If the substrate temperature is low enough, adatoms may have insufficient energy to diffuse and react or be emitted into vacuum. These adatoms will be codeposited with the compound film as crystal defects or as a second phase. As a result of these competing processes, the growth rate and composition of the deposited film vary depending on the incident flux from each source, the energy of the incident species, and the substrate temperature.

Model Equations

In this section, model equations are developed using steady state component and overall mass balances that account for all incident, adsorbed, emitted, and reflected species. Constitutive equations providing a quantitative description of the rate processes are presented. The material- and process-specific model parameters that must be obtained from the literature or through experiment are described. No equipment-specific fitting parameters are needed.

Mass balances

The steady state component balances for the control volume at the surface of the growing film as shown in Figure 2 are:

$$\frac{1}{\phi Mw(j)}\frac{dMj}{dt} = r(i,j) - r(r,j) - r(e,j) - r(rxt,j) \quad (1)$$

where j represents each of the components in the reacting system. For example, in the (CdZn)S material system, six components are considered: Cd, Zn, S, CdS, ZnS, and (CdZn)S. If compound sources are used, then the molecular beams will consist of monatomic cadmium and zinc and diatomic sulfur (Jackson, 1984). Elemental sources, however, form beams of monatomic cadmium and zinc and polyatomic sulfur, S_n, where the number of sulfur atoms, n, depends on the operating temperature and pressure of the source (Mills, 1974). For typical conditions reported in this work S_6, S_7, and S_8 are the predominate

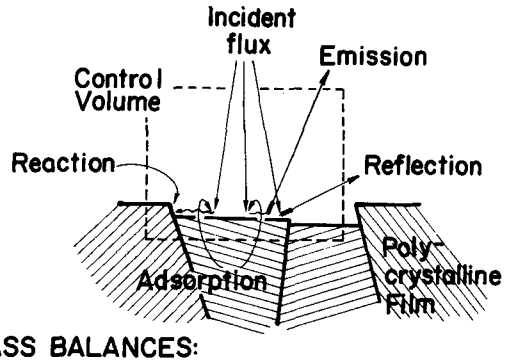

MASS BALANCES:

Accumulation of component j, kg moles/m²/sec
r(d,j)=

+r(i,j)~Incident rate of j, kg moles/m²/sec
-r(r,j)~Reflection rate of j, kg moles/m²/sec
-r(e,j)~Emission rate of j, kg moles/m²/sec
-r(rxt,j)~Reaction rate of j, kg moles/m²/sec

Figure 2. Control volume at surface of a growing film and basic mass balance showing accumulation terms.

species. For compound films [CdS, ZnS, (CdZn)S in the solid phase], the component balances are used to account for the stoichiometry of the film. They do not represent the structure of the film nor do they imply the existence of single molecules of CdS or ZnS in the solid or adsorbed phase.

The lefthand side of Eq. 1 represents the molar rate of accumulation or deposition of adsorbed component j per unit area (ϕ):

$$r(d,j) = \frac{1}{\phi Mw(j)} \frac{dMj}{dt} \tag{2}$$

Equation 1 is based on a control volume small enough that the incident flux from each source is uniform within it. The net rate of surface diffusion into the control volume is assumed to be negligible compared to this incident flux. The incident component $r(i,j)$ is either adsorbed or reflected from the surface where the rate of reflection is $r(r,j)$. The adsorbed component may react at a rate $r(rxt,j)$ to form a compound, be emitted from the surface into vacuum at a rate $r(e,j)$, or be codeposited with the compound in an elemental form at a rate $r(d,j)$. Solutions of Eq. 1 with appropriate constitutive rate expressions for $r(i,j)$, $r(r,j)$, $r(e,j)$, and $r(rxt,j)$ for all components within the control volume yield the deposition rate and composition of the film as a function of the component incident rates or fluxes, the temperature of the incident species, and the substrate temperature.

Constitutive relationships

Incident Flux. The incident flux rate of each component can be measured independently or be calculated using previously verified models (Jackson et al., 1985; Rocheleau et al., 1982). The rate at which the material leaves the control volume is controlled by two mechanisms, reflection $r(r,j)$, and emission of the adsorbed species into vacuum $r(e,j)$, as indicated in Figure 2.

Adsorption-Reflection. The incomplete adsorption of an incident component is characterized by the reflection factor δ (Hirth and Pound, 1960; Eyring et al., 1964; Hirth, 1966). The reflection rate can be assumed to be proportional to the incident rate:

$$r(r,j) = [1 - \delta(j)]r(i,j) \tag{3}$$

where $\delta(j)$ is the reflection factor of incident component j.

The reflection factor is weakly dependent on the temperatures of the substrate and the incident molecule. It also depends on the composition of the deposited film (Eyring t al., 1964). By definition $\delta(j)$ must be between zero and one. In practice, the reflection factor of one component of a compound film can be determined experimentally by using an excess flux of the second component from an elemental source (Smith and Pickhardt, 1975).

Emission. The rate at which the adsorbed components are emitted from the substrate back into vacuum, $r(e,j)$, depends on the composition of the surface, expressed as the adatom concentration $[j^a]$, the binding energy of the adatom to the substrate and the thermal energy of the adatom:

$$r(e,j) = Ev(j)[j^a] \tag{4}$$

The emission factor, $Ev(j)$, characterizes the binding energy to the substrate and the thermal energy of the adatom. The emission factors are component-specific and may depend on the species present as an adatom, e.g., S_2 vs. S_8. As will be shown below, it is not necessary to evaluate the value of the emission factor since it is lumped together with the forward reaction rate constant.

Reaction. An adsorbed species may react to form the binary or ternary alloy semiconductor, may be emitted into vacuum, or may be codeposited as a second phase. In order to simplify the equations that follow, a one-to-one stoichiometry for the reaction step is assumed. This assumption is applicable to the II-VI and III-V classes of compounds. However, by assuming other stoichiometries the model can be applied to any class of compounds. Equation 5 shows the net reaction for the formation of a solid phase ternary alloy film of $(A_{1-x}B_x)Y$ allowing for the codeposition of the element Y:

$$(1 - x)A^a + xB^a + (1 + \lambda)Y^a \rightarrow (A_{1-x}B_x)Y + \lambda Y \tag{5}$$

The coefficient x in Eq. 5 is zero for deposition of a binary semiconductor AY. If codeposition of a second elemental phase does not occur, then λ is also zero. The ability to predict codeposition of an element is particularly important for low vapor pressure materials like tellurium during the formation of HgTe or when there is a large incident flux rate of one element.

The ternary alloy $A_{1-x}B_xY$ shown in Eq. 5 is modeled as a random mixture of $(1 - x)AY$ plus xBY. Constitutive equations for the formation of AY and BY, described by Eq. 5, are derived by assuming that the kinetic expressions are governed by two competing, parallel surface reactions:

$$(1 - x)A^a + (1 - x)Y^a \underset{k_r(AY)}{\overset{k_f(AY)}{\rightleftharpoons}} (1 - x)AY \tag{6}$$

$$xB^a + xY^a \underset{k_r(BY)}{\overset{k_f(BY)}{\rightleftharpoons}} xBY \tag{7}$$

The net reaction rates for species A, B, Y, AY, and BY are then represented by:

$$r(rxt, A) = k_f(AY)[A^a]^n[Y^a]^m - (1 - x)k_r(AY) \quad (8)$$

$$r(rxt, B) = k_f(BY)[B^a]^n[Y^a]^m - xk_r(BY) \quad (9)$$

$$r(rxt, Y) = r(rxt, A) + r(rxt, B) \quad (10)$$

$$r(rxt, AY) = -r(rxt, A) \quad (11)$$

$$r(rxt, BY) = -r(rxt, B) \quad (12)$$

where:

$k_f(AY)$, $k_f(BY)$ = The forward reaction rate constants for the formation of the AY and BY compounds, respectively.
$k_r(AY)$, $k_r(BY)$ = The reverse reaction rate constants for the formation of the AY and BY compounds, respectively, $kmol/m^2 \cdot s$ or $(no./cm^2/s)$.
n, m = Order of the reaction with respect to each component. Value is on the order of 1.0.

The factors $(1 - x)$ and x in Eqs. 8 and 9 account for the decrease of the net reverse reaction rate with the composition of the film relative to the pure compounds due to the effective surface coverage with AY or BY, respectively. Large changes in the energetics in the process would be seen by changes in k_f with surface composition. Equations 8 and 9 are similar to the surface reaction step proposed by Somarjai and Jepsen (1964) for the evaporation of CdS, and are similar to the interaction probability theory for the deposition of compound semiconductors proposed by Freller and Gunther (1982).

As shown in Eqs. 6–9, the reaction rate is described by two kinetic constants, the forward rate constant k_f, and the reverse rate constant k_r. In this model the forward and reverse rate constants are assumed to have the usual Arrhenius form:

$$k_r \quad \text{or} \quad k_f = k' \exp\left[-E/(R_o T_s)\right] \quad (13)$$

For most compounds of interest, including many II-VI and III-V semiconductors (Somerjai and Jepsen, 1964) the dissociation of the compound to form the adsorbed elemental species is the rate-controlled step during evaporation. The reverse reaction only becomes important at high substrate temperatures where dissociative evaporation of the compound is significant.

Codeposition of Second Phase. A second elemental phase is formed if the adsorption rate of the incident flux, $\delta(j)r(i, j)$, is greater than the sum of the reaction rate $r(rxt, j)$, Eqs. 8–12, and the emission rate $r(e, j)$. The emission rate of the element is then assigned a maximum value given by the Hertz-Knudsen equation:

$$r(e_{max}, j) = P(T_a, j)\alpha_v(j)[2\pi R_o T_a Mw(j)]^{-1/2} \quad (14)$$

where:

$P(T_a, j)$ = Vapor pressure of element j at the adatom temperature, Pa $(dynes/cm^2)$
$\alpha_v(j)$ = Evaporation coefficient for the element j
T_a = Adatom temperature, K
R_o = Gas law constant
$Mw(j)$ = Molecular weight of species, j

This expression, Eq. 14, was successfully used with the other model equations to accurately predict deposition conditions where codeposition of Te occurs for the (CdHg)Te material system.

Application of the Model

In this section the model equations are solved for three material systems, (CdZn)S, (CdHg)Te, and $CuInSe_2$. Specific assumptions, the model equations, and values of the model parameters are listed for each system. The model predictions are shown to agree closely with experimental behavior.

(CdZn)S

The key assumptions used to simplify the model, Eqs. 1–14, for the (CdZn)S material system are the following.

1. The incident and reflected flux of the compound components are zero:

$$r(i, \text{CdS}) = r(i, \text{ZnS}) = 0 \quad (15)$$

$$r(r, \text{CdS}) = r(r, \text{ZnS}) = 0 \quad (16)$$

Compound and elemental sources have been used for (CdZn)S depositions. In either case, only elemental species exist in the incident flux since the compounds dissociatively evaporate and the rate of forming the compound species in the space between the source and substrate is negligible at the vacuums used.

2. CdS and ZnS are known to evaporate dissociatively; therefore, their rate of emission into vacuum is zero:

$$r(e, \text{CdS}) = r(e, \text{ZnS}) = 0 \quad (17)$$

3. The three elements, Cd, Zn, and S, are reasonably volatile at the substrate temperatures (200–260°C) and incident fluxes of interest. Consequently, it is assumed that they are not deposited as an elemental phase with the compound film:

$$r(d, \text{Cd}) = r(d, \text{Zn}) = r(d, \text{S}) = 0 \quad (18)$$

At substrate temperatures below ~180°C or an excess incident flux of $>50 \times 10^{-8}$ $kmol/m^2 \cdot s$ of the least volatile component, zinc, elemental deposition is likely. Equations dealing with codeposition have been applied to (CdHg)Te system and are discussed below.

4. At the substrate temperature of interest, the reverse reaction rate is negligible:

$$k_r(\text{CdS}) = k_r(\text{ZnS}) = 0 \quad (19)$$

At substrate temperatures >300°C, dissociation of the compound—i.e., the reverse reaction rate—becomes important, as evidenced by the rate of dissociative evaporation.

Substituting these assumptions, Eqs. 15–19, into the model, Eqs. 1–14, and simplifying gives a system of four simultaneous equations; these, Eqs. 20–23, are shown at the top of Table 1 along with condition Eqs. 24 and 25.

Three sets of experiments were done to verify the model equations and determine values of the model parameters: cadmium sulfide depositions, zinc sulfide depositions, and depositions of the ternary alloy, cadmium-zinc sulfide. In each experiment the

Table 1. (CdZn)S Deposition Model Equations and Parameters

Equations		
$r(d, \text{CdS}) = K(\text{CdS})\,[\delta(\text{Cd})\,r(i, \text{Cd}) - r(d, \text{CdS})]^n \times [\delta(\text{S})\,r(i, \text{S}) - r[d, (\text{CdZn})\text{S}]]^m$		(20)
$r(d, \text{ZnS}) = K(\text{ZnS})\,[\delta(\text{Zn})\,r(i, \text{Zn}) - r[d, \text{ZnS}]]^n \times [\delta(\text{S})\,r(i, \text{S}) - r[d, (\text{CdZn})\text{S}]]^m$		(21)
$r[d, (\text{CdZn})\text{S}] = r[(d, \text{CdS}) + r(d, \text{ZnS})$		(22)
$x = r(d, \text{ZnS})/r[d, (\text{CdZn})\text{S}]$		(23)
where		
$K(\text{CdS}) = k_f(\text{CdS})/Ev(\text{Cd})^n/Ev(\text{S})^m$		(24)
$K(\text{ZnS}) = k_f(\text{ZnS})/Ev(\text{Zn})^n/Ev(\text{S})^m$		(25)

Parameter	Value	Deposition Conditions
δ(Cd)	0.8–0.9	T_s = 200–260°C T_l = 430–460°C
δ(Zn)	0.6–0.7	T_s = 200–260°C T_l = 534–577°C
δ(S)	0.5–0.7	T_s = 200–260°C T_l = 167–172°C
n, m	½ or 1	T_s = 200–260°C x = 0.0–1.0
K(ZnS), K(CdS)		
for $n = m = 1$	$>10^8$ m² · s/kmol	T_s = 200–260°C
for $n = m = ½$	>10 (dimensionless)	x = 0.0–1.0
$K(\text{ZnS})/K(\text{CdS})$		
for $n = m = 1$	~16	T_s = 200–220°C
for $n = m = ½$	~4	x = 0.1–0.9

deposition rate $r[d, (\text{CdZn})\text{S}]$ and zinc fraction x were measured as a function of the incident flux composition and substrate temperature. A nonlinear least-squares procedure was used to fit the model predictions to the experimental data. The model was considered accurate if the calculated goodness of fit of the model from the nonlinear least-squares program was equal to the estimated experimental error for both the film composition, x, and the deposition rate, $r(d, \text{CdS})$, $r(d, \text{ZnS})$, or $r[d, (\text{CdZn})\text{S}]$. These criteria were met. The resulting estimated values of the model parameters are shown in Table 1. The solution of the model equations is discussed more fully elsewhere (Jackson, 1984).

A convenient way to present the results for CdS and ZnS depositions is to plot the deposition rates, $r(d, \text{CdS})$ or $r(d, \text{ZnS})$, as a function of the incident flux rate of one element while fixing the incident flux rate of the second elemental component. This type of plot is shown in Figure 3 for the deposition of ZnS as a function of the sulfur incident flux rate for a substrate temperature of 200°C. Experimental data points and curves representing the best-fit model predictions are shown for each of four different zinc incident flux rates. Near the origin of the graph, the film growth rate is proportional to the sulfur incident rate, $r(i, \text{S})$. The slope in this region is approximately equal to the value of the sulfur reflection factor obtained from the least-squares analysis. Thus, in the sulfur-limited regime, the growth rate is described by

$$r(d, \text{ZnS}) \sim \delta(\text{S})r(i, \text{S}) \tag{26}$$

where

$$\delta(\text{S}) \sim 0.5 \tag{27}$$

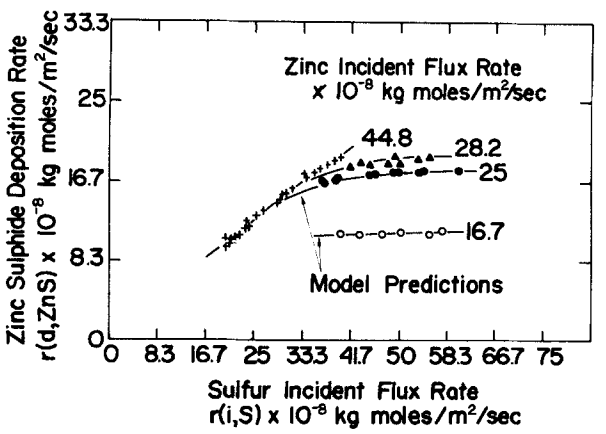

Figure 3. Dependence of ZnS deposition rate on sulfur incident flux rate.
Substrate temp., 200°C; no incident Cd

Similarly, at a high sulfur incident flux rate the deposition rate becomes independent of the sulfur flux rate. Where the curves are horizontal in Figure 3, the deposition rate is ~70% of the zinc incident rate, a fraction that is very close to the Zn reflection factor. An expression analogous to Eq. 26 is then applicable in this regime:

$$r(d, \text{ZnS}) \sim \delta(\text{Zn})r(i, \text{Zn}) \tag{28}$$

where

$$\delta(\text{Zn}) \sim 0.7 \tag{29}$$

The close agreement between the limiting slopes determined graphically from the sulfur- and zinc-rich regimes and the numerically determined reflection factors indicates that the deposition rate in these regimes is limited by the rate at which the low incident flux component is adsorbed onto the substrate.

Not only does the model accurately predict the sulfur- and zinc-limited regimes, it also accurately predicts the transition or knee in the curves shown in Figure 3. At the knee in the curves, the rate of deposition is controlled by the rates at which the adsorbed zinc and sulfur react. The curvature of the bend depends on the speed of the reaction relative to the emittance rate of the elemental components. For a very fast reaction, the curvature is very sharp, as is the case in Figure 3, indicating that the deposition is limited by the adsorption rate of one of the components. From the CdS and ZnS depositions, only an approximate or minimum value for the apparent reaction rate constants K(CdS) and K(ZnS), can be estimated. Further, since it is a very fast reaction, the orders of the reaction, n and m, cannot be accurately estimated from this data. Minimum values of K(CdS) and K(ZnS) are shown in Table 1 for two values of n and m.

For the alloy depositions, the goodness of fit was again equal to the estimated experimental error for both the film composition x, and deposition rate $r[d, (\text{CdZn})\text{S}]$. Excellent agreement between the predicted film composition and measured film composition for the alloy film is shown in Figure 4. The predicted composition is within 3 atomic percent of the measured composition across the range of composition from 10 to 90 atomic percent. The values of the model parameters used for these pre-

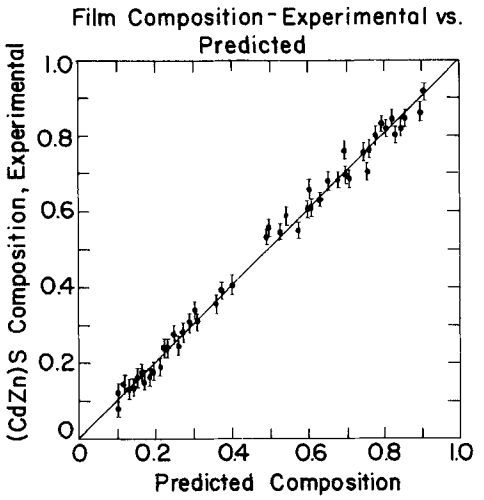

Figure 4. Comparison of measured and predicted Zn fraction x in $(Cd_{1-x}Zn_x)S$ alloy films.

dictions agreed with those obtained for the CdS and ZnS depositions. In addition, the data from the alloy depositions show that the zinc reacts faster than the cadmium so that the ratio of the apparent rate constants for ZnS to CdS is greater than one. The ratio resulting from the numerical fit is shown in Table 1.

During development of the model, several alternate rate expressions were tried for the rate of reaction step, Eqs. 8–12. These included a Langmuir-Hinshelwood-Hougen-Watson expression (Carberry, 1976) as well as an interaction probability relationship first proposed by Gunther (1968). However, none of these was able to model the strong asymptotic behavior of the data. The strong asymptotic behavior shown in Figure 3 has been reported by others, including Smith and Pickhardt (1975), and Foxon (1983) for other II-VI and III-V compounds. This suggests that the model may be applicable to wide classes of compounds formed by physical vapor deposition techniques.

(HgCd)Te

Several assumptions, similar to those used for the (CdZn)S material system, are used to simplify the model for the (HgCd)Te material system. These include the following.

1. The incident and reflected flux of the compound components are zero:

$$r(i, \text{HgTe}) = r(i, \text{CdTe}) = 0 \tag{30}$$

$$r(r, \text{HgTe}) = r(r, \text{CdTe}) = 0 \tag{31}$$

As in the (CdZn)S system both compound and elemental sources have been used for (CdZn)S depositions. In either case, only elemental species exist in the incident flux since the compounds dissociatively evaporate and the rate of forming the compound species in the space between the source and substrate is negligible.

2. HgTe and CdTe are known to evaporate dissociatively; therefore, the rate of emission into vacuum is zero:

$$r(e, \text{HgTe}) = r(e, \text{CdTe}) = 0 \tag{32}$$

3. The metal components, Cd and Hg, are much more volatile than tellurium. Consequently, it is assumed that they are not deposited as an elemental phase with the compound film:

$$r(d, \text{Hg}) = r(d, \text{Cd}) = 0 \tag{33}$$

Tellurium, however, has such a low volatility that it can form a second elemental phase in the compound film. Consequently, Eq. 14 must be used to estimate the emission rate if an elemental phase forms.

Substituting these assumptions, Eqs. 30–33, into the model and simplifying gives a system of simultaneous equations, Eqs. 34–43, shown in Table 2. Equations 34–40 are nearly identical to those used for the (CdZn)S system, Table 1, except that the reverse reaction rates, k_r(HgTe) and k_r(CdTe), have been included. Equations 41–43 are used to account for codeposition of elemental tellurium. One important feature of Eqs. 41–43 is that the maximum emission rate of tellurium, $r(e_{max}, \text{Te})$ must be evaluated at the adatom temperature, T_a. The adatom temperature depends on the energy or temperature of the incident tellurium, T_i, the substrate temperature, T_s, and the ability of the substrate to accommodate the energy of the incident species. The thermal characteristics of the substrate were modeled using a thermal accommodation coefficient, ϵ, shown in Eq. 42.

The values of the model parameters shown in Table 2 were estimated using physical property data from Mills (1974) and experimental data as discussed elsewhere (Baron and Jackson 1986).

The conversion of CdTe predicted by the model and measured experimentally is shown as a function of substrate temperature and incident flux rate from a compound CdTe source in Figure

Table 2. (HgCd)Te Deposition Model Equations and Parameters

Equations		
$r(d, \text{CdTe}) = K(\text{CdTe})\, r(e, \text{Cd})^n\, r(e, \text{Te})^m - (1 - x)\, k_r(\text{CdTe})$		(34)
$r(d, \text{HgTe}) = K(\text{HgTe})\, r(e, \text{Hg})^n\, r(e, \text{Te})^m - x\, k_r(\text{HgTe})$		(35)
$r(e, \text{Cd}) = \delta(\text{Cd})\, r(i. \text{Cd}) - r(d, \text{CdTe})$		(36)
$r(e, \text{Hg}) = \delta(\text{Hg})\, r(i, \text{Hg}) - r(d, \text{HgTe})$		(37)
$r(d, (\text{HgCd})\text{Te}) = r(d, \text{CdTe}) + r(d, \text{HgTe})$		(38)
$x = r(d, \text{HgTe})/r[d, (\text{HgCd})\text{Te}]$		(39)
For no tellurium codeposition		
$r(e, \text{Te}) = \delta(\text{Te})\, r(i, \text{Te}) - r[d, (\text{HgCd})\text{Te}]$		(40)
For tellurium deposition		
$r(e, \text{Te}) = r(e_{\text{max}}, \text{Te}) = P_o(T_a, \text{Te})\, \alpha_v(\text{Te})\, [2\pi R_o T_a Mw(\text{Te})]^{-1/2}$		(41)
$T_a = (1 - \epsilon)\, T_s + \epsilon T_i$		(42)
$r(d, \text{Te}) = \delta(\text{Te})\, r(i, \text{Te}) - r[d, (\text{HgCd})\text{Te}] - r(e_{\text{max}}, \text{Te})$		(43)
Parameter	Value or Expression	Units
δ(Cd), δ(Hg), δ(Te)	0.9	—
$r(e_{\text{max}}, \text{Te})$	$\frac{3.0 \times 10^7}{\sqrt{T_a}} \exp(-17{,}715/T_a)$	kmol/m² · s
K(CdTe)	$5.7 \times 10^{-3} \exp(3{,}390/T_s)$	—
K(HgTe)	$2.7 \times 10^{-5} \exp(5{,}100/T_s)$	—
k_r(CdTe)	$\frac{2.8 \times 10^7}{\sqrt{T_s}} \exp(-23{,}030/T_s)$	kmol/m² · s
k_r(HgTe)	$\frac{1.2 \times 10^7}{\sqrt{T_s}} \exp(-13{,}980/T_s)$	kmol/m² · s
n, m	½	—
ϵ	0.88	—

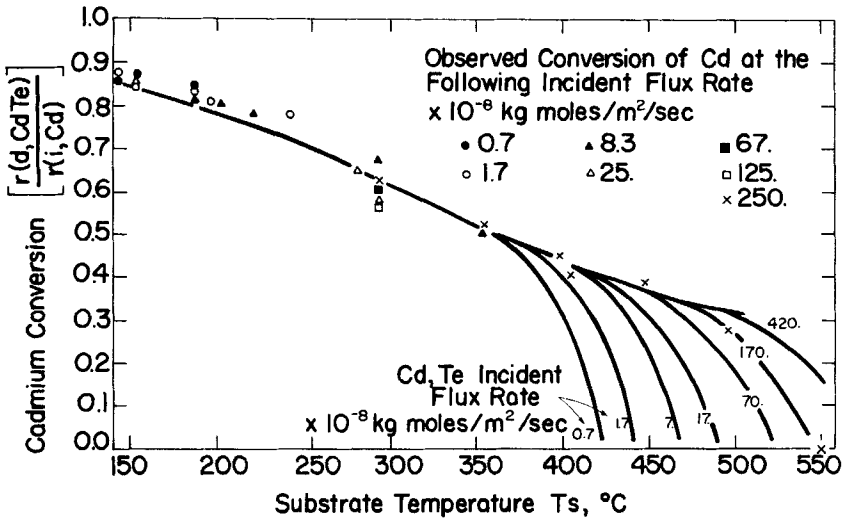

Figure 5. Measured and predicted (solid curves) conversion of Cd as a function of substrate temperature and incident flux rate from a compound CdTe source.

5. The conversion of CdTe is defined as:

$$\eta(\mathrm{CdTe}) = \frac{r(d, \mathrm{CdTe})}{r(i)} \tag{44}$$

The incident flux rates of Cd or Te, $r(i)$, are equal for a compound source as considered in this example. For substrate temperatures from 100 to 350°C, the CdTe conversion changes from 0.9 to 0.5 and is independent of the incident flux. This decrease in the CdTe conversion with the substrate temperature is a result of the greater emission of the adsorbed elemental components at higher substrate temperatures. The insensitivity of the conversion with the incident flux below 350°C is accurately predicted as long as the orders of the reaction with respect to Cd and Te, n and m, are equal to ½. Above 350°C the reverse reaction rate, k_r(CdTe), becomes significant and the CdTe conversion drops rapidly with increasing substrate temperature and becomes dependent on the incident flux. This predicted trend is in part verified by the data.

The effect of varying deposition conditions including the substrate temperature, incident flux rate from a compound CdTe source, and the incident flux temperature on the codeposition of elemental tellurium is shown in Figure 6. The solid lines represent the predicted atomic fraction of tellurium deposited as a second phase in the CdTe film. The source temperature or incident flux temperature, T_i, needed to generate the flux rate indicated is shown at the top of the graph. The open circles represent films deposited at the conditions shown for which no tellurium was observed by X-ray diffraction. The crosses represent conditions for which elemental tellurium, >0.02 atomic fraction, was detected.

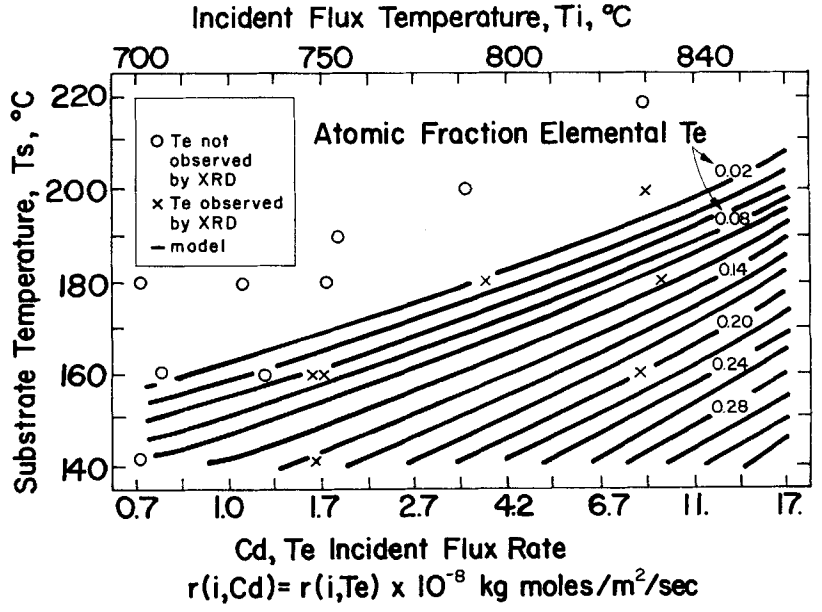

Figure 6. Evaporation conditions yielding codeposited elemental Te using a compound CdTe source.

The experimental data points indicate that elemental deposits of tellurium are formed preferentially at lower substrate temperatures and/or higher incident fluxes. For example, at a substrate temperature of 180°C, elemental deposits were not detected below an incident flux of 1.7×10^{-8} kmol/m^2 · s but were formed above a flux of 4×10^{-8} kmol/m^2 · s. This is in good agreement with the model predictions. The model predicts that at low substrate temperatures CdTe can be deposited without codepositing tellurium, provided that the incident flux and therefore the surface concentration of the adsorbed tellurium is low enough. At high substrate temperatures, adsorbed tellurium is emitted into vacuum more readily from the surface, and consequently a much higher incident flux is required for elemental codeposition.

The model equations were extended to the deposition of (HgCd)Te with the results shown in Figures 7 and 8. The solid lines represent the model behavior using the parameters shown in Table 2. The points are data reported by Faurie et al. (1983). The data were obtained at a constant cadmium and tellurium flux of 1.7×10^{-8} kmol/m^2 · s.

Figure 7 shows the Hg conversion as a function of substrate temperature and mercury flux. The Hg conversion is defined as:

$$\eta(\mathrm{Hg}) \equiv \frac{r(d, \mathrm{HgTe})}{r(i, \mathrm{Hg})} \tag{45}$$

where $r(d, \mathrm{HgTe})$ is the rate at which HgTe is deposited in the (HgCd)Te alloy film. The numbers next to the points indicate the experimental incident fluxes estimated by Faurie (1985).

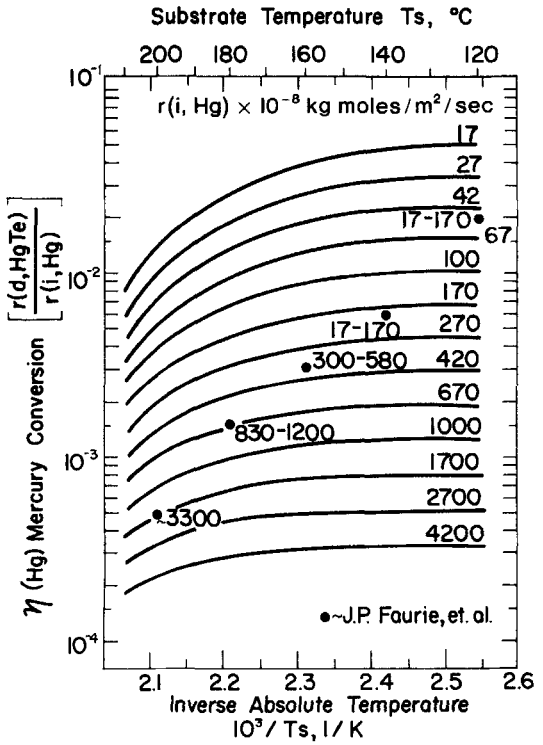

Figure 7. Hg conversion as a function of Hg incident flux rate $r(i, \mathrm{Hg})$, and substrate temperature T_s for HgTe deposited in (HgCd)Te alloy.
Data of Faurie et al. (1985)

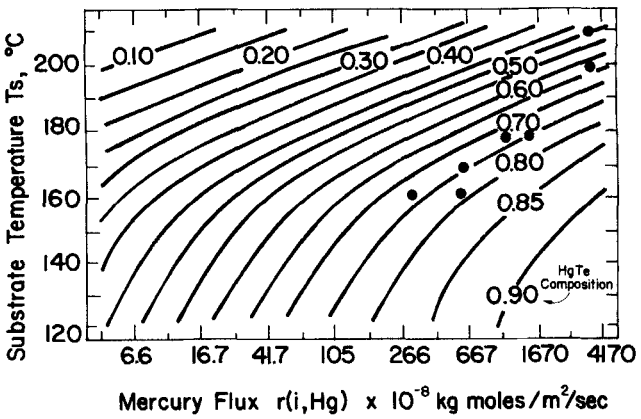

Figure 8. Mole fraction of HgTe deposited in (HgCd)Te alloy as a function of Hg incident flux rate and substrate temperature.
Data of Faurie et al. (1983)

The model predictions are shown as lines of constant mercury flux. As expected, the model predicts a drop in the Hg conversion with an increase in substrate temperature and an increase in the Hg flux. Although the experimental data are not at a constant Hg flux, the data do show a decrease in the Hg conversion with an increased flux and substrate temperature that is consistent with the model predictions.

Figure 8 shows the influence of substrate temperature and mercury flux on the HgTe content of the (HgCd)Te film. The points represent conditions reported by Faurie et al. (1985) that formed (HgCd)Te films with 80% HgTe. The curves, representing the model predictions, show a decrease in the HgTe composition as the substrate temperature increases or the mercury flux decreases. This predicted trend agrees closely with the experimental points. The quantitative agreement is very good except at the highest Hg flux.

$CuInSe_2$

The $CuInSe_2$ material, unlike (CdHg)Te or (CdZn)S, is not an alloy, as shown by its equilibrium phase diagram (Palatnik and Rugacheva, 1967). Several investigators (Don et al., 1985; Stolt et al., 1985) have noticed that the film compositions grown from elemental sources in a vacuum evaporation system appear to lie along a pseudobinary tie line between Cu_2Se and In_2Se_3 with $CuInSe_2$ at the midpoint of this tie line. Another observation used in the assumptions that follow is that Se_2 and In_2Se are the predominate species volatilized from In_2Se_3 and $CuInSe_2$ (Mills, 1974; Lamereaux et al., 1983). Based on these observations the following constraints and assumptions are used to simplify the model equations.

1. The selenium incident flux is in excess relative to copper or indium:

$$r(i, \mathrm{Se}) \gg r(i, \mathrm{Cu}) + r(i, \mathrm{In}) \tag{46}$$

This is a constraint rather than an assumption, and reflects the fact that copper and indium are so involatile that without an excess flux of selenium, elemental deposits of copper and indium would form.

2. The incident and reflected flux of the compounds Cu_2Se,

In_2Se_3, and $CuInSe_2$ are zero:

$$r(i, Cu_2Se) = r(i, In_2Se_3) = r(i, CuInSe_2) = 0 \quad (47)$$

$$r(r, Cu_2Se) = r(r, In_2Se_3) = r(r, CuInSe_2) = 0 \quad (48)$$

Unlike the (CdZn)S and (HgCd)Te material systems, only elemental evaporation sources have been successfully used for $CuInSe_2$ depositions (Michelsen and Chen, 1980; Birkmire et al., 1984). Because of this and the fact that the rate of forming the compound species in the vacuums used is negligible, only elemental species exist in the incident flux.

3. The rate of emission of the compound components Cu_2Se, In_2Se_3, and $CuInSe_2$ are negligible:

$$r(e, Cu_2Se) = r(e, In_2Se_3) = r(e, CuInSe_2) = 0 \quad (49)$$

These components either do not exist as adsorbed single molecules or they undergo dissociative evaporation.

4. All the copper that is adsorbed, $\delta(Cu)\, r(i, Cu)$, reacts to form a selenide compound:

$$r(rxt, Cu) = \delta(Cu) r(i, Cu) \quad (50)$$

This is a result of the excess selenium and the highly favorable reaction to form either of the selenide compounds, Cu_2Se or $CuInSe_2$.

5. All the indium that is adsorbed, $\delta(In) r(i, In)$, reacts to form a selenide compound and is subsequently deposited or is emitted as In_2Se:

$$\delta(In) r(i, In) = r(rxt, In) - 2r(e, In_2Se) \quad (51)$$

This results from the use of excess selenium, the favorable reaction to form the selenide compounds, and is consistent with observations (Mills, 1974; Lamereaux et al., 1983) that In_2Se is volatile at the temperatures of interest (~400°C).

6. The rate of formation of adsorbed In_2Se is governed by two reversible reactions that are at equilibrium:

a. For $Cu_2Se(s) + CuInSe_2(s)$ two-phase mixture:

$$2CuInSe_2(s) \xleftrightarrow{K(CuInSe_2)} Cu_2Se(s) + In_2Se^a + Se_2^a \quad (52)$$

where

$$K(CuInSe_2) \equiv r(e, Se) r(e, In_2Se) \quad (53a)$$

$$K(CuInSe_2) \alpha [Se_2^a][In_2Se^a] \quad (53b)$$

b. For $In_2Se_3(s) + CuInSe_2(s)$ two-phase mixture:

$$In_2Se_3(s) \xleftrightarrow{K(In_2Se_3)} In_2Se^a + Se_2^a \quad (54)$$

where

$$K(In_2Se_3) \equiv r(e, Se) r(e, In_2Se) \quad (55a)$$

$$K(In_2Se_3) \alpha [Se_2^a][In_2Se^a] \quad (55b)$$

and

$$K(In_2Se_3) > K(CuInSe_2)$$

7. $CuInSe_2$ is assumed to be a pseudobinary formed from equal amounts of $Cu_2Se + In_2Se_3$:

a. If $r(rxt, Cu) > r(rxt, In)$ then (56)

$$r(d, CuInSe_2) = r(rxt, In) \quad (57)$$

$$r(d, Cu_2Se) = \tfrac{1}{2}[r(rxt, Cu) - r(rxt, In)] \quad (58)$$

$$r(d, In_2Se_3) = 0 \quad (59)$$

b. If $r(rxt, In) > r(rxt, Cu)$ then (60)

$$r(d, CuInSe_2) = r(rxt, Cu) \quad (61)$$

$$r(d, Cu_2Se) = 0 \quad (62)$$

$$r(d, In_2Se_3) = \tfrac{1}{2}[r(rxt, In) - r(rxt, Cu)] \quad (63)$$

c. If $r(rxt, In) = r(rxt, Cu)$ then (64)

$$r(d, CuInSe_2) = r(rxt, Cu) \quad (65)$$

$$r(d, Cu_2Se) = 0 \quad (66)$$

$$r(d, In_2Se_3) = 0 \quad (67)$$

Table 3. $CuInSe_2$ Deposition Model Equations and Parameters

Equations	
$r(rxt, Cu) = \delta(Cu)\, r(i, Cu)$	(50)
$r(rxt, In) = \delta(In)\, r(i, In) - 2\, r(e, In_2Se)$	(51)
$r(rxt, Se) = \tfrac{1}{2} r(rxt, Cu) + \tfrac{3}{2} r(rxt, In)$	(68)
$r(e, Se) = \delta(Se)\, r(i, Se) - r(rxt, Se) - r(e, In_2Se)$	(69)
If $Cu_2Se(s) + CuInSe_2(s)$ two-phase mixture is formed	
$r(e, In_2Se) = K(CuInSe_2)/r(e, Se)$	(70)
$r(rxt, Cu) > r(rxt, In)$	(56)
$r(d, CuInSe_2) = r(rxt, In)$	(57)
$r(d, Cu_2Se) = \tfrac{1}{2}[r(rxt, Cu) - r(rxt, In)]$	(58)
$r(d, In_2Se_3) = 0$	(59)
If $In_2Se_3(s) + CuInSe_2(s)$ two-phase mixture is formed	
$r(e, In_3Se) = K(In_2Se_3)/r(e, Se)$	(71)
$r(rxt, In) > r(rxt, Cu)$	(60)
$r(d, CuInSe_2) = r(rxt, Cu)$	(61)
$r(d, Cu_2Se) = 0$	(62)
$r(d, In_2Se_3) = \tfrac{1}{2}[r(rxt, In) - r(rxt, Cu)]$	(63)
If single-phase $CuInSe_2(s)$ is formed	
$K(CuInSe_2)/r(e, Se) < r(e, In_2Se) < K(In_2Se_3)/r(e, Se)$	(72)
$r(rxt, In) = r(rxt, Cu)$	(64)
$r(d, CuInSe_2) = r(rxt, Cu)$	(65)
$r(d, Cu_2Se) = 0$	(66)
$r(d, In_2Se_3) = 0$	(67)

Parameters	Value	Units
$\delta(Cu), \delta(In), \delta(Se)$	0.9	—
$K(CuInSe_2)$	8.3×10^6 $10^{[7,630(1/673 - 1/(T_s+673))]}$	kmol/m² · s
$K(In_2Se_3)$	5.8×10^7 $10^{[7,630(1/673 - 1/(T_s+673))]}$	kmol/m² · s

Substituting these assumptions and simplifications, Eqs. 46–67, into the model and simplifying gives the set of equations shown in Table 3. Although these equations appear dissimilar to those used in the (CdZn)S and (HgCd)Te material systems, they were derived using the same basic mass balances and assuming the same underlying rate processes: adsorption-reflection, emission, and reaction. The model parameters were either set to some reasonable value (the reflection factors equal to 0.9), or were adjusted to give reasonable agreement to available data (Thornton et al., 1984).

Figure 9 shows the overall composition and the conditions necessary to form single-phae $CuInSe_2$. The predictions were calculated for the experimental conditions used to generate the data of Thornton et al. (1984) shown in the inset of Figure 9. There is close agreement between the predicted and measured film compositions. Further, several trends predicted by the model are verified by the data. Specifically, the single-phase $CuInSe_2$ field appears at copper incident flux rates, $r(i, Cu)$, that are less than the indium incident flux rate. This is a result of the emission of In_2Se from the film. The relative composition of copper to indium is larger in the film than it is in the incident flux. For example, at a copper incident flux rate of 2.7×10^{-8} kmol/m^2 · s, corresponding to a copper to indium flux ratio of 0.53, the copper to indium ratio in the film is one. This reflects the fact that In_2Se is less likely to be emitted from $CuInSe_2$ than from In_2Se_3.

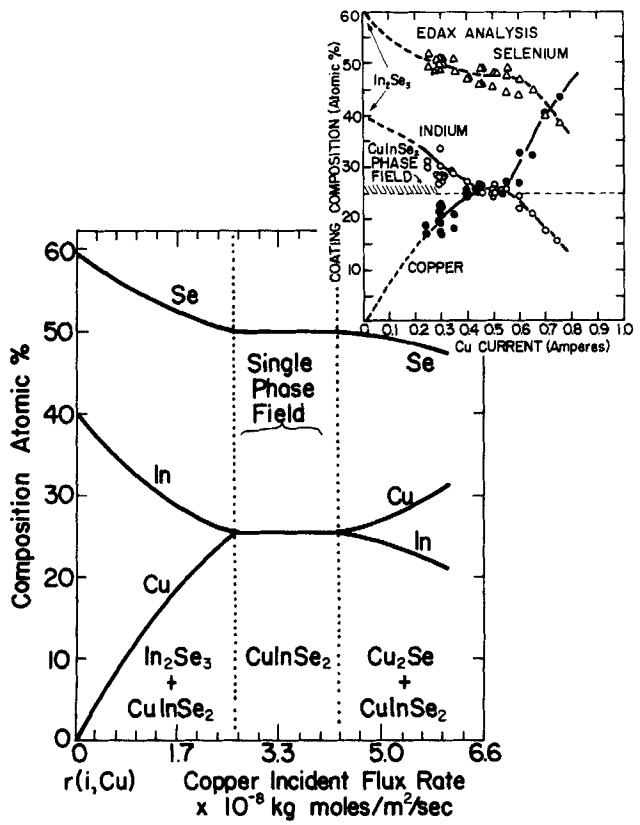

Figure 9. Effect of Cu incident flux on predicted and observed $CuInSe_2$ composition.
Data of Thornton et al. (1984).
Substrate temp., ~400°C
$r(i, In)$ 5×10^{-8} kmol/m^2 · s
$r(i, Se)$ 1.7×10^{-8} kmol/m^2 · s

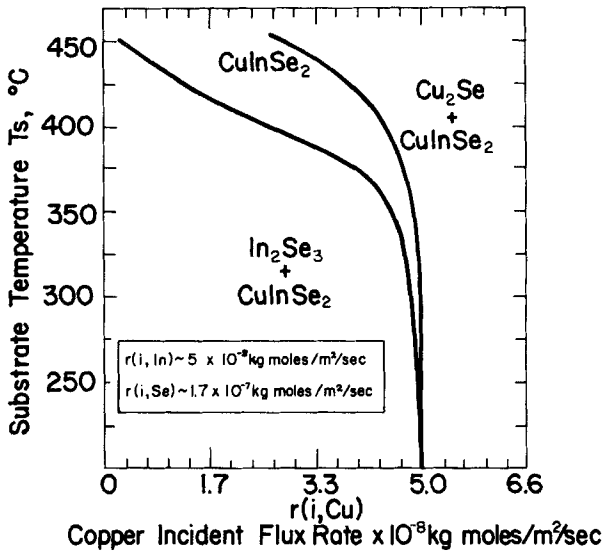

Figure 10. Predicted $CuInSe_2$ single-phase field as a function of substrate temperature and Cu incident flux.

Figure 10 shows how the predicted single-phase $CuInSe_2$ field is shifted with substrate temperature. This field widens and shifts to a lower copper incident flux rate as the substrate temperature is increased. This is consistent with the observation of Michelsen and Chen (1980) and Birkmire et al. (1984) that a lower amount of copper, relative to indium, is required when substrate temperatures are shifted from 350 to 450°C in order to produce device quality (single-phase) $CuInSe_2$ material.

Conclusions

Model equations based on the principle of mass conservation and appropriate constitutive relations have been developed to provide a mathematical description of the physical vapor deposition of a number of important semiconductor films, including (CdZn)S, (HgCd)Te, and $CuInSe_2$. The model predicts the growth rate, alloy composition, and conditions where codeposition of an elemental or second compound phase occurs. The model predictions were shown to agree with available data over a wide range of deposition conditions for all three material systems. The model has, for the first time, quantified several important experimental observations including: the effects of substrate temperature and incident flux on the conversion of incident species, and on the composition of an alloy (Figures 3, 4, 5, 7, and 8); the conditions where an element is codeposited with the compound (Figure 6); and the deposition conditions needed to grow single or multiple compound phases in a film (Figures 9 and 10).

The agreement of the model with the wide range of available data make the model useful for the analysis of bench-scale experiments and the design of large-scale systems. Despite the agreement between the model and available experimental observations, more data are needed to verify the model over a wider parameter space and refine the estimates of the model parameters.

Notation

A, B = arbitrary elemental species from column II or III of the Periodic Table

E = activation energy of the forward reaction rate constant, Eq. 13, J, kcal/mol, ergs, or eV
$Ev(j)$ = emission factor, Eq. 4, 1/s
j = arbitrary elemental or compound species
$[j^a]$ = surface concentration of adsorbed adatoms, kmol/m^2 or no./cm^2
$K(AY)$ = apparent reaction rate constant, Eqs. 24, 25
$k_f(AY)$, $k_f(BY)$ = true forward reaction rate constant for the formation of AY and BY compounds
$k_r(AY)$, $k_r(BY)$ = reverse reaction rate constants for AY and BY compounds, kmol/m^2/s
k' = preexponential factor for reaction rate constants, Eq. 13
m, n = order of compound formation reaction with respect to each component
Mj = mass of component j in control volume, kg or g
$Mw(j)$ = molecular weight, kg/kmol, g/gmol, or g/no.
$P(T_a, j)$, $P(T_s, j)$ = vapor pressure of species j evaluated at adatom temperature or substrate temperature, Pa, dynes/cm^2
R_o = gas law constant
$r(d, j)$ = deposition rate or rate of accumulation of component j inside control volume, kmol/m^2 · s, no./cm^2 · s
$r(e, j)$ = rate of emission of component j from control volume, kmol/m^2 · s, no./cm^2 · s
$r(e_{max}, j)$ = maximum rate of emission of component j, Eq. 14, kmol/m^2 · sec, no./cm^2 · s
$r(i, j)$ = rate of incident flux of component j into control volume, kmol/m^2 · sec, no./cm^2 · s
$r(rxt, j)$ = rate of reaction of component j within control volume, kmol/m^2 · sec, no./cm^2 · s
$r(r, j)$ = rate of reflection of component j within control volume, kmol/m^2 · sec, no./cm^2 · s
T_a, T_s = adatom and substrate temperatures, K
T_i = temperature of incident beam
t = time, s
x = composition of ternary alloy, atomic fraction
Y = arbitrary elemental component for column V or VI of the Periodic Table

Greek letters

$\alpha_v(j)$, α_v = evaporation coefficient of component j
$\delta(j)$, δ = reflection factors
ϵ = thermal accommodation coefficient, Eq. 42
λ = relative amount of an element codeposited in a film, Eq. 5
η = material conversion, Eqs. 44, 45
ϕ = surface area covered by control volume, m^2 or cm^2

Literature cited

Baron, B. N., and S. C. Jackson, "Fundamental Engineering Analysis of CdTe/CdS Photovoltaic Processing, Final Report," SERI Subcontract XL-4-03146-1, Jan. 1986, SERI Pub. No. SERI/STR-211-2970 (1986).

Birkmire, R. W., R. B. Hall, and J. E. Phillips, "Material Requirements for High-Efficiency $CuInSe_2$/CdS Solar Cells," *17th IEEE PV Specialists Conf.* Orlando, 882 (1984).

Brody, T. P., "The Thin Film Transistor—A Late Flowering Bloom," *IEEE Trans. Electronic Dev.*, **180-3**(11), 1614 (1984).

Bunshah, R. F., et al., *Deposition Technologies for Films and Coatings Developments and Applications*, Noyes, Park Ridge, NJ (1982).

Carberry, J. J., *Chemical and Catalytic Reaction Engineering*, McGraw-Hill, New York, 382–394 (1976).

Chow, P. P., and D. Johnson, "Growth and Characterization of MBE-Grown HgTe-CdTe Superlattices," *J. Vac. Sci. Tech.*, **A3**(1), 67 (1985).

Dayton, B. B., "Gas Flow Patterns at Entrance and Exit of Cylindrical Tubes," *Trans. 2nd Amer. Vacuum Soc. Vac. Symp.*, **5**, 5 (1961).

Don, E. R., S. J. Russell, and R. Hill, "RHEED Studies of $CuInSe_2$ Epitaxial Films," *18th IEEE PV Specialists Conf.*, Las Vegas, 1060 (1985).

Eyring, H., F. M. Wanlass, and E. M. Eyring, Chap. 1, *Condensation and Evaporation of Solids*, E. Rutner, P. Goldfinger, and J. P. Hirth, eds., Gordon and Breach, New York (1964).

Faurie, J. P., private communication (Oct., 1985).

Faurie, J. P., A. Million, R. Boch, and J. L. Tissot, "Latest Developments in the Growth of $Cd_xHg_{1-x}Te$ and CdTe-HgTe Superlattices by Molecular Beam Epitaxy," *J. Vac. Sci. Tech.*, **A1**(3), 1593 (1983).

Faurie, J. P., M. Boukircbe, J. Reno, S. Stranantban, and C. Hsu, "Molecular Beam Epitaxy of Alloys and Superlattices Involving Mercury," *J. Vac. Sci. Tech.*, **A3**(1), 55 (1985).

Foxon, C. T., "MBE Growth of GaAs and III-V Alloys," *J. Vac. Sci. Tech.*, **B1**(2), 293 (1983).

Freller, H., and K. G. Gunther, "Three-Temperature Method as an Origin of Molecular Beam Epitaxy," *Thin Solid Films*, **88**, 291 (1982).

Giordmaine, J. A., and T. C. Wang, "Molecular Beam Formation by Long Parallel Tubes," *J. Appl. Phys.*, **31**, 463 (1960).

Gunther, K. G., *The Use of Thin Films in Physical Investigations*, J. C. Anderson, ed. Academic Press, New York, 213–231 (1968).

Hirth, J. P., Chap. 5, *Vapor Deposition*, C. F. Powell, J. H. Oxles, and J. M. Blocher, eds., Wiley, New York (1966).

Hirth, J. P., and G. H. Pound, "Coefficients of Evaporation and Condensation," *J. Phys. Chem.*, **64**, 619 (1960).

Jackson, S. C., "Engineering Analysis of the Deposition of Cadmium-Zinc Sulfide Semiconductor Film," Ph.D. Diss., Univ. Delaware, Newark (1984).

Jackson, S. C., B. N. Baron, R. E. Rocheleau, and T. W. F. Russell, "Molecular Beam Distribution from High Rate Sources," *J. Vac. Sci. Tech.*, **A3**(5), 1916 (1985).

Jansen, F., and A. R. Melnyk. "The Evaporation and Condensation of As_2Se_3-like Materials," *J. Vac. Sci. Tech.*, **A2**(3), 1248 (1984).

Kawabe, M., and N. Matsiura, "Preferential Desorption of Ga from Al_xGa_{1-x} as Grown by Molecualr Beam Epitaxy," *Japan J. Appl. Phys.*, **23**(6), L351 (1984).

Lamereaux, R. H., K. H. Lau, and R. D. Brittain, "High-Temperature Equilibrium Studies of Copper Indium Selenide," Final Report SERI Subcontract XZ-2-02001 (Mar. 4, 1983).

Michelsen, R. A., and W. S. Chen, "High Photocurrent Polycrystalline Thin-Film CdS/$CuInSe_2$ Solar Cell," *Appl. Phys. Lett.*, **36**, 371, (1980).

Mills, K. C., *Thermodynamic Data for Inorganic Sulphides, Selenides, and Tellurides*, Butterworth, London (1974).

Mino, N., M. Kobayashi, M. Konagai, and K. Takahashi, "Epitaxial Growth of High-Quality ZnSe on Si Substrates by Molecular Beam Epitaxy and Application to DC Electroluminescent Cells," *J. Appl. Phys.*, **58**(2), 793 (1985).

Myers, T. H., A. W. Waltner, and J. F. Schetzinor, "Properties of CdTe-Te Alloy Films Prepared Using Molecular Beams," *J. Appl. Phys.*, **53**(8), 5697 (1982).

Palatnik, L. S., and E. R. Rogacheva "Phase Diagrams and Structure of Some Semiconductor $A_2^{I}C^{VI}$-$B_2^{III}C^{VI}$ Alloys," *Sov. Phys. Dok.*, **12**, 503 (1967).

Rocheleau, R. E., B. N. Baron, and T. W. F. Russell, "Analysis of Evaporation of Cadmium Sulfide for Manufacture of Solar Cells," *AIChE J.*, **28**, 656 (1982).

Russell, T. W. F., B. N. Baron, and R. E. Rocheleau, "Fundamentals and Application of Solar Energy. II," *AIChE Symp. Ser.*, **S-210** (1979).

Smith, D. L., and V. Y. Pickhardt, "Molecular Beam Epitaxy of II-VI Compounds," *J. Appl. Phys.*, **46**(6), 2366 (1975).

Somerjai, G. A., and D. W. Jepsen, "Evaporation Mechanism of CdS Single Crystals. I: Surface Concentration and Temperature Dependence of the Evaporation Rate," *J. Chem. Phys.*, **41**(5), 1389 (1964).

Stickney, R. E., and R. F. Keating, S. Yamamoto, and W. J. Hastings, "Angular Distributions of Flow from Orifices and Tubes at High Knudsen Numbers," *J. Vac. Sci. Tech.*, **4**(1), 10 (1968).

Stolt, L., M. Jargelius, J. Hedstrom, D. Sigurd, and E. Niemi, "Growth of $CuInSe_2$ Thin Films," *18th IEEE PV Specialists Conf.*, Las Vegas, 1047 (1985).

Summers, C. J., E. L. Meeks, and N. W. Cox, "Molecular Beam Epitaxial Growth of CdTe, HgTe, and $Hg_{1-x}CdXTe$ Alloys," *J. Vac. Sci. Tech.*, **B2**(2), 224 (1984).

Thornton, J. A., D. G. Cerneg, R. B. Hall, S. P. Shea, and J. D. Meakin, "Reactive Sputtered Copper Indium Diselenide Films for Photovoltaic Applications," *J. Vac. Sci. Tech.*, **A2**(2), 307 (1984).

Manuscript received Feb. 11, 1986, and revision received Oct. 27, 1986.